

# Randomness in infinitesimal extent in the McLerran-Venugopalan model

Kenji Fukushima

*Yukawa Institute for Theoretical Physics, Kyoto University, Kyoto 606-8502, Japan*

We study discrepancy between the analytical formulation and the numerical implementation of the McLerran-Venugopalan (MV) model. The infinitesimal extent of a fast-moving nucleus should retain longitudinal randomness in the color source distribution even when the longitudinal extent approximates zero due to the Lorentz contraction, which is properly taken into account in the analytical treatment. We point out that longitudinal randomness is lost in numerical simulations because of lack of the infinitesimal path-ordering along the longitudinal direction. We quantitatively investigate how much the results with and without longitudinal randomness differ from each other. We finally mention on physical implication to the MV model analyses on the early-time dynamics in the relativistic heavy-ion collisions.

PACS numbers: 24.85.+p, 12.38.-t, 25.75.-q

## I. INTRODUCTION

It is a tempting idea to approximate the wavefunction of an interacting particle by mediating gauge fields surrounding the particle. Such a description of a fast-moving charged particle by virtual photons is long known as the Weizsäcker-Williams approximation. If we apply this idea to the strong interaction, we can approximately give the wavefunction of a heavy hadron by gluon fields which extend from the local color distribution inside the hadron. The formalism of the Color Glass Condensate (CGC) can accommodate the non-Abelian extension of the Weizsäcker-Williams approximation [1, 2].

The CGC formalism aims to embody the parton saturation picture arising as a result of the small- $x$  evolution at high energies [3]. The geometric scaling beautifully indicates the existence of the saturation scale as a function of Bjorken's  $x$  [4]. The CGC formalism has been forming an important building-block of high-energy Quantum Chromodynamics (QCD). If we further make a Gaussian approximation for distribution of the random color source and fix its dispersion by the saturation scale [5], we reach the McLerran-Venugopalan (MV) model [1].

So far, the MV model has been well examined analytically in the case of a light projectile (e.g. a color dipole, a proton, etc) scattering off a dense CGC target [6, 7, 8, 9, 10, 11, 12]. The scattering problem of two CGC objects, i.e. high-energy nucleus-nucleus collision [13, 14, 15, 16, 17] is hard to solve analytically, however, and the possible analysis is limited to the numerical method [18, 19, 20, 21, 22]. Only the initial fields right after the collision are analytically available in a simple form [13, 18, 23]. The initial chromo-electric and chromo-magnetic fields are thus calculable by means of the proper Gaussian average over the color source distribution [17, 21].

In this work we will address a problem that the numerical formulation of the MV model has significant difference from the analytical description. We will clarify the physical meaning of difference between the analytical and the numerical prescriptions. The crucial point is that the formulation involves two distinct limits in the longitudinal direction; one is vanishing extent of a nucleus and the other is vanishing correlation length in the random color distribution. We will then quantify how much the numerical results turn out to underestimate the expectation value of the initial fields as compared to the analytical answer.

## II. MCLERRAN-VENUGOPALAN MODEL

If we have two sources which represent particles moving fast in the positive and negative  $z$ -directions (“right” and “left” respectively), we can write the corresponding current using the light-cone coordinates as

$$J^\mu = \delta^{\mu+} \rho^{(1)}(\mathbf{x}_\perp, x^-) + \delta^{\mu-} \rho^{(2)}(\mathbf{x}_\perp, x^+), \quad (1)$$

where we dropped  $x^+$ -dependence in the right-moving source and  $x^-$ -dependence in the left-moving source as usual because of the Lorentz time dilatation. Then, converting the coordinates from the light-cone variables  $x^\pm$  to the proper-time  $\tau$  and the rapidity  $\eta$  which are related by  $x^\pm = (\tau/\sqrt{2})e^{\pm\eta}$ , we can express the initial fields right after two nuclei collide as [13, 23, 24]

$$\begin{aligned} E^\eta &= ig \left( [\alpha_1^{(1)}, \alpha_1^{(2)}] + [\alpha_2^{(1)}, \alpha_2^{(2)}] \right), \\ B^\eta &= ig \left( [\alpha_1^{(1)}, \alpha_2^{(2)}] + [\alpha_1^{(2)}, \alpha_2^{(1)}] \right), \end{aligned} \quad (2)$$

and the transverse fields  $(E^i, B^i)$  are zero [21], under the assumption that  $\rho^{(1)}(\mathbf{x}_\perp, x^-)$  and  $\rho^{(2)}(\mathbf{x}_\perp, x^+)$  behave like  $\delta(x^-)$  and  $\delta(x^+)$  respectively near the light cone [14]. This assumption is the case because of the Lorentz contraction when two nuclei travel at the speed of light. In the above, the color matrices,  $\alpha_i^{(n)}$ 's, are the gauge field configurations in the radial gauge,  $A_\tau \propto x^- A^+ + x^+ A^- = 0$ , created from each color source  $\rho^{(n)}$ . The solution must satisfy  $\partial_i \alpha_i^{(n)} = -\rho^{(n)}$  with a constraint that  $\alpha_i^{(n)}$  takes a pure gauge form so that its field strength is vanishing.

The covariant gauge is most convenient to get an explicit solution. By rotating the obtained solution in the covariant gauge to the radial gauge, we can write down the desirable solution as [6];

$$\alpha_i^{(1)}(\mathbf{x}_\perp, x^-) = -\frac{1}{ig} V(\mathbf{x}_\perp, x^-) \partial_i V^\dagger(\mathbf{x}_\perp, x^-), \quad \alpha_i^{(2)}(\mathbf{x}_\perp, x^+) = -\frac{1}{ig} W(\mathbf{x}_\perp, x^+) \partial_i W^\dagger(\mathbf{x}_\perp, x^+), \quad (3)$$

where the gauge rotation matrices are

$$\begin{aligned} V^\dagger(\mathbf{x}_\perp, x^-) &= \mathcal{P}_{x^-} \exp \left[ ig \int_{-\infty}^{x^-} dz^- \int d^2 \mathbf{y}_\perp G_0(\mathbf{x}_\perp - \mathbf{y}_\perp) \tilde{\rho}^{(1)}(\mathbf{y}_\perp, z^-) \right], \\ W^\dagger(\mathbf{x}_\perp, x^+) &= \mathcal{P}_{x^+} \exp \left[ ig \int_{-\infty}^{x^+} dz^+ \int d^2 \mathbf{y}_\perp G_0(\mathbf{x}_\perp - \mathbf{y}_\perp) \tilde{\rho}^{(2)}(\mathbf{y}_\perp, z^+) \right]. \end{aligned} \quad (4)$$

Here  $\mathcal{P}_{x^\pm}$  denotes the path-ordering with respect to  $x^\pm$ . We remark that  $\tilde{\rho}$  in Eq. (4) is the color source in the covariant gauge that is not identical to original  $\rho$  in the radial gauge. Since the Gaussian weight is a gauge-invariant function of  $\text{tr}[\rho^2] = \text{tr}[\tilde{\rho}^2]$  (see Eq. (7)), we do not have to discriminate  $\rho$  and  $\tilde{\rho}$ . We will thus not use the tilde any more but just write  $\rho$  regardless of gauge choices. The two-dimensional massless propagator is defined by  $\partial_\perp^2 G_0(\mathbf{x}_\perp) = -\delta^{(2)}(\mathbf{x}_\perp)$  which is singular in both the infrared and the ultraviolet sectors. Let  $a$  and  $L$  be the lattice spacing and the number of the lattice sites, and then we can express  $G_0(\mathbf{x}_\perp)$  in the lattice regularization as

$$G_0(\mathbf{x}_\perp) = \frac{1}{2L^2} \sum_{n_i=1-L/2}^{L/2} \frac{\exp[i(x_1 2\pi n_1 / La + x_2 2\pi n_2 / La)]}{2 - \cos(2\pi n_1 / L) - \cos(2\pi n_2 / L)}. \quad (5)$$

The summation is supposed to exclude a singular point  $n_1 = n_2 = 0$  because we impose the global color neutrality  $\rho^{(n)}(\mathbf{p}_\perp = 0) = 0$  and then the singular point  $n_1 = n_2 = 0$  does not appear at all in Eq. (4). It is easy to check that Eq. (5) is reduced to the standard expression,  $G_0(\mathbf{x}_\perp) \rightarrow \int d^2 \mathbf{p}_\perp e^{i\mathbf{x}_\perp \cdot \mathbf{p}_\perp} / [(2\pi)^2 \mathbf{p}_\perp^2]$ , in the continuum limit where  $a \rightarrow 0$  and  $L \rightarrow \infty$ .

The later-time dynamics is uniquely determined by the equation of motion with the initial fields given by Eq. (2). Any physical observables are therefore given in terms of  $V$  and  $W$  in principle, which we shall denote as  $\mathcal{O}[V, W]$  generally. We can compute the expectation value by taking the average,

$$\langle \mathcal{O}[V, W] \rangle = \int [d\rho^{(1)}][d\rho^{(2)}] \mathcal{W}^{(1)}[\rho^{(1)}] \mathcal{W}^{(2)}[\rho^{(2)}] \mathcal{O}[V, W], \quad (6)$$

with the Gaussian weight,

$$\begin{aligned} \mathcal{W}^{(1)}[\rho^{(1)}] &= \exp \left[ - \int dx^- d^2 \mathbf{x}_\perp \frac{\text{tr}[\rho^{(1)}(\mathbf{x}_\perp, x^-)^2]}{g^2 [\mu^{(1)}(x^-)]^2} \right], \\ \mathcal{W}^{(2)}[\rho^{(2)}] &= \exp \left[ - \int dx^+ d^2 \mathbf{x}_\perp \frac{\text{tr}[\rho^{(2)}(\mathbf{x}_\perp, x^+)^2]}{g^2 [\mu^{(2)}(x^+)]^2} \right]. \end{aligned} \quad (7)$$

The normalization of the color trace is understood as  $\text{tr}[t^m t^n] = \frac{1}{2} \delta^{mn}$ , where  $t^m$ 's are the  $\text{SU}(N_c)$  algebra in the fundamental representation. The scale  $\mu^{(1)}(x^-)$  and thus  $\rho^{(1)}(\mathbf{x}_\perp, x^-)$  (or  $\mu^{(2)}(x^+)$  and thus  $\rho^{(2)}(\mathbf{x}_\perp, x^+)$ ) may have finite extent in the  $x^-$  (or  $x^+$  respectively) direction because the Lorentz  $\gamma$ -factor is finite in fact and also because small- $x$  components should extend in the longitudinal direction.

If we are interested in evaluating the initial energy density,  $\mathcal{O}[V, W]$  should be  $\text{tr}[(E^\eta)^2 + (B^\eta)^2]$ , that is [17, 22],

$$\epsilon_0 = \langle \text{tr}[(E^\eta)^2 + (B^\eta)^2] \rangle = 2N_c(N_c^2 - 1) \langle \alpha^{(1)} \alpha^{(1)} \rangle \langle \alpha^{(2)} \alpha^{(2)} \rangle. \quad (8)$$

where we introduced a notation to indicate the diagonal component, i.e.  $\langle \alpha_i^a \alpha_j^b \rangle = \delta_{ij} \delta^{ab} \langle \alpha \alpha \rangle$  for  $\alpha^{(1)}$  and  $\alpha^{(2)}$  respectively. We will use this notation again when we show the numerical results later.

### III. QUESTION

In the numerical implementation, for practical reasons, it is difficult to compute the expectation value of the Wilson lines (4) as they are. In the first approximation the longitudinal finiteness is only negligible as compared to the transverse size and one can take the following limit;

$$\rho^{(1)}(\mathbf{x}_\perp, x^-) \rightarrow \bar{\rho}^{(1)}(\mathbf{x}_\perp) \delta(x^-), \quad \rho^{(2)}(\mathbf{x}_\perp, x^+) \rightarrow \bar{\rho}^{(2)}(\mathbf{x}_\perp) \delta(x^+). \quad (9)$$

Then one might anticipate that all physical quantities are given as a function of the integrated scale,

$$[\bar{\mu}^{(1)}]^2 = \int_{-\infty}^{\infty} dx^- [\mu^{(1)}(x^-)]^2, \quad [\bar{\mu}^{(2)}]^2 = \int_{-\infty}^{\infty} dx^+ [\mu^{(2)}(x^+)]^2. \quad (10)$$

As a matter of fact, we can verify this expectation in the analytical evaluation associated with only one source [8, 9, 12], that is, only  $[\bar{\mu}^{(1)}]^2$  (or  $[\mu^{(2)}]^2$ ) appears in the Gaussian average of a function of  $V$  (or  $W$ ) alone with the weight  $\mathcal{W}^{(1)}[\rho^{(1)}]$  (or  $\mathcal{W}^{(2)}[\rho^{(2)}]$  respectively).

In the prevailing numerical formulation the Wilson lines (4) simplify approximately under the limit (9);

$$\begin{aligned} V^\dagger(\mathbf{x}_\perp, x^-) &\stackrel{?}{\rightarrow} \bar{V}^\dagger(\mathbf{x}_\perp, x^-) = \exp \left[ ig \int d^2 \mathbf{y}_\perp G_0(\mathbf{x}_\perp - \mathbf{y}_\perp) \bar{\rho}^{(1)}(\mathbf{y}_\perp) \theta(x^-) \right], \\ W^\dagger(\mathbf{x}_\perp, x^+) &\stackrel{?}{\rightarrow} \bar{W}^\dagger(\mathbf{x}_\perp, x^+) = \exp \left[ ig \int d^2 \mathbf{y}_\perp G_0(\mathbf{x}_\perp - \mathbf{y}_\perp) \bar{\rho}^{(2)}(\mathbf{y}_\perp) \theta(x^+) \right]. \end{aligned} \quad (11)$$

These would be, of course, exact if there were not for the path-ordering  $\mathcal{P}_{x^\pm}$ . The question we are addressing in the present paper is the validity of this naive prescription (11).

### IV. FORMULATION

Let us focus only on the  $V$ -sector in what follows because the initial energy density is factorized into the  $V$ -sector and the  $W$ -sector as seen in Eq. (8) and exactly the same argument works for the  $W$ -sector as well. For simple notation, then, we shall omit the superscript (1) which indicates the right mover.

The subtle point comes from the fact that another Dirac delta function is involved implicitly besides Eq. (9). Namely, the Gaussian weight (7) leads to the following correlation function;

$$\langle \rho_a(\mathbf{x}_\perp, x^-) \rho_b(\mathbf{y}_\perp, y^-) \rangle = g^2 [\mu(x^-)]^2 \delta^{ab} \delta(\mathbf{x}_\perp - \mathbf{y}_\perp) \delta(x^- - y^-). \quad (12)$$

We need to deal with two  $\delta(x^-)$ 's properly in order to formulate the problem in question in an appropriate way. For this goal it is convenient to introduce a regularization to the longitudinal Dirac delta functions. We modify the Wilson line accordingly as

$$V_\epsilon^\dagger(\mathbf{x}_\perp, x^-) = \mathcal{P}_{x^-} \exp \left[ ig \int_{-\infty}^{x^-} dz^- \int d^2 \mathbf{y}_\perp G_0(\mathbf{x}_\perp - \mathbf{y}_\perp) \rho_\epsilon(\mathbf{x}_\perp, z^-) \right], \quad (13)$$

where the regularized color source must satisfy

$$\lim_{\epsilon \rightarrow 0} \rho_\epsilon(\mathbf{x}_\perp, x^-) = \bar{\rho}(\mathbf{x}_\perp) \delta(x^-). \quad (14)$$

We shall introduce another regularization for the correlation function in a way as

$$\langle \rho_a(\mathbf{x}_\perp, x^-) \rho_b(\mathbf{y}_\perp, y^-) \rangle_\zeta = g^2 [\mu(x^-)]^2 \delta^{ab} \delta(\mathbf{x}_\perp - \mathbf{y}_\perp) \delta_\zeta(x^- - y^-), \quad (15)$$

such that the regularized delta function must satisfy

$$\lim_{\zeta \rightarrow 0} \delta_\zeta(z^-) = \delta(z^-). \quad (16)$$

We are now ready to elaborate the question in a more sophisticated manner. The replacement in Eq. (11) realizes if  $\epsilon \rightarrow 0$  comes first before  $\zeta \rightarrow 0$ . In the analytical calculation, on the other hand, the relevant limit is  $\zeta \rightarrow 0$  followed by  $\epsilon \rightarrow 0$  later. Thus, a mathematically sensible description of the question should be

$$\lim_{\zeta \rightarrow 0} \lim_{\epsilon \rightarrow 0} \langle \mathcal{O}[V_\epsilon] \rangle_\zeta \stackrel{?}{=} \lim_{\epsilon \rightarrow 0} \lim_{\zeta \rightarrow 0} \langle \mathcal{O}[V_\epsilon] \rangle_\zeta. \quad (17)$$

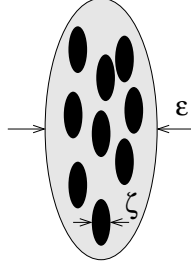


FIG. 1: Schematic picture of a nucleus with two regulators  $\epsilon$  and  $\zeta$ . Intuitively  $\epsilon$  signifies the longitudinal extent of the whole nucleus and  $\zeta$  represents the longitudinal correlation length inside the nucleus. If randomness of the color source distribution is attributed to color confinement in each nucleon,  $\zeta$  corresponds to the longitudinal extent of the nucleon.

Here, the left-hand side corresponds to the numerical implementation (11) and the right-hand side corresponds to the analytical one.

We sketch the intuitive interpretation of  $\epsilon$  and  $\zeta$  in Fig. 1. Roughly speaking,  $\epsilon$  is the longitudinal extent of a fast-moving nucleus and  $\zeta$  is the correlation length of the color distribution inside the nucleus. The physical limit should keep  $\epsilon > \zeta$  as is the case in the right-hand side of the question (17). If  $\epsilon$  goes to zero first, the longitudinal structure of randomness is lost. Then only one infinitesimal “sheet” of the two-dimensional random distribution is left and the path-ordering becomes irrelevant (see also Fig. 4). The numerical prescription (11) assumes such unphysical ordering of two noncommutative limits.

## V. RESULTS

We will explicitly confirm that the order of two limits is noncommutative indeed. We will begin with the simplest case of the tadpole expectation value. Then we will proceed to the case of the gauge fields which is directly related to the estimate for the initial energy density by Eq. (8).

### A. Tadpole

In the simplest case of the tadpole operator, i.e.  $\mathcal{O}[V] = V^\dagger$ , we can make a quick comparison even without resorting to the numerical method. We already know the analytical answer for the right-hand side of Eq. (17). That is given by [9, 12]

$$\lim_{\epsilon \rightarrow 0} \lim_{\zeta \rightarrow 0} \langle V_\epsilon^\dagger \rangle_\zeta = \exp \left[ -g^4 \bar{\mu}^2 \frac{N_c^2 - 1}{4N_c} L(0, 0) \right], \quad (18)$$

where  $L(0, 0)$  is the notation in Ref. [9] which is defined as

$$L(0, 0) = \int d^2 \mathbf{x}_\perp G_0(\mathbf{x}_\perp) G_0(\mathbf{x}_\perp) = \frac{a^2}{4L^2} \sum_{n_i=1-L/2}^{L/2} \frac{1}{[2 - \cos(2\pi n_1/L) - \cos(2\pi n_2/L)]^2} \simeq \frac{0.962a^2}{2\pi} \left( \frac{L}{2\pi} \right)^2. \quad (19)$$

Here, as in Eq. (5), the zero-mode ( $n_1 = n_2 = 0$ ) is to be removed by neutrality. The quadratic form approximates the sum quite well with a coefficient 0.962 that we find numerically.

As for the left-hand side of the question (17), we have to perform the following Gaussian integral;

$$\lim_{\zeta \rightarrow 0} \lim_{\epsilon \rightarrow 0} \langle V_\epsilon^\dagger \rangle_\zeta = \int [d\bar{\rho}] \exp \left[ ig \int d^2 \mathbf{y}_\perp G_0(\mathbf{x}_\perp - \mathbf{y}_\perp) \bar{\rho}(\mathbf{y}_\perp) \right] \exp \left[ - \int d^2 \mathbf{x}_\perp \frac{\text{tr}[\bar{\rho}(\mathbf{x}_\perp)^2]}{g^2 \bar{\mu}^2} \right]. \quad (20)$$

It should be mentioned that the first exponential is a matrix, which makes the Gaussian integral difficult. Although it is a tough calculation for arbitrary  $\text{SU}(N_c)$  group, the  $\text{SU}(2)$  case ( $N_c = 2$ ) is feasible immediately because the exponential of  $\text{SU}(2)$  matrices is easily manipulated. After some calculations we find that the above Gaussian integral results in

$$\lim_{\zeta \rightarrow 0} \lim_{\epsilon \rightarrow 0} \langle V_\epsilon^\dagger \rangle_\zeta = \left( 1 - g^4 \bar{\mu}^2 \frac{1}{4} L(0, 0) \right) \exp \left[ -g^4 \bar{\mu}^2 \frac{1}{8} L(0, 0) \right], \quad (21)$$

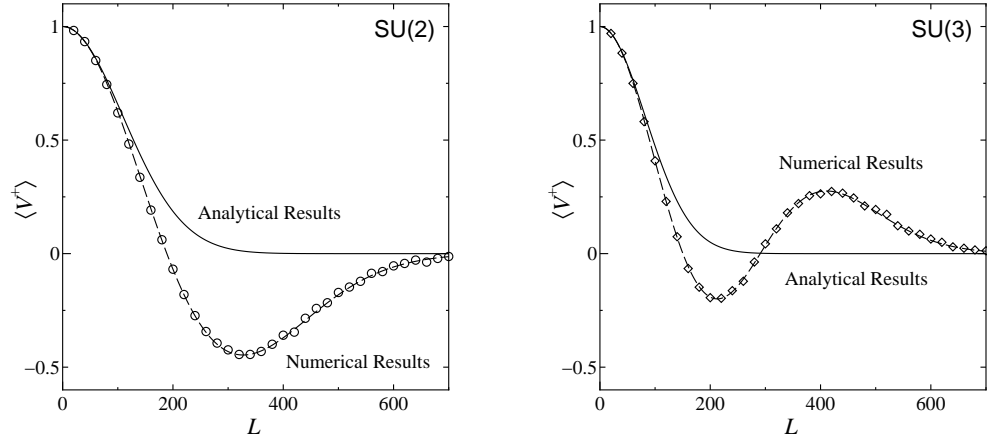


FIG. 2: Tadpole expectation value as a function of  $L$  with the parameter choice  $g^2\bar{\mu}a = 0.17$ . The left figure is for the SU(2) group and the right for the SU(3) group. The solid curves represent the analytical results by Eq. (18). The open circles represent the numerical results by the Monte-Carlo integration. The thin dashed curves show Eq. (21) in the SU(2) case and Eq. (25) in the SU(3) case, respectively. The SU(2) and SU(3) numerical data agree well with the thin dashed curves, which means that our Monte-Carlo integration works nicely.

which obviously differs from Eq. (18) with  $N_c = 2$  substituted;

$$\lim_{\epsilon \rightarrow 0} \lim_{\zeta \rightarrow 0} \langle V_\epsilon^\dagger(\mathbf{x}_\perp) \rangle_\zeta = \exp \left[ -g^4 \bar{\mu}^2 \frac{3}{8} L(0, 0) \right]. \quad (22)$$

It is interesting to see from the above that Eq. (21) can be a good approximation to Eq. (22) as long as  $g^2\bar{\mu}aL$  is small enough to allow for the Taylor expansion.

It should be instructive to compute Eq. (20) numerically in the Monte-Carlo integration though we already have the answer. In order to compare to the existing numerical calculations in literatures, we shall adopt the parameter choice same as used in Ref. [22]. That is,

$$\frac{g^2}{4\pi} = \frac{1}{\pi}, \quad g^2\bar{\mu}a = 0.17, \quad L = 700, \quad (23)$$

was chosen in Ref. [22] and then the nucleus size is given by

$$R_A = \frac{aL}{\sqrt{\pi}}. \quad (24)$$

We change the value of  $L$  to see the functional form. Therefore, if we increase  $L$  while keeping  $g^2\bar{\mu}a$  fixed at 0.17, the nucleus size or the infrared cut-off  $R_A$  grows up in proportion to  $L$ .

We plot the analytical formula (18) as a function of  $L$  by the solid curve for the SU(2) case in the left of Fig. 2 and the SU(3) case in the right of Fig. 2. Since  $g^2\bar{\mu}a$  is a constant, what Fig. 2 means is the  $R_A$ -dependence of the tadpole expectation value. The open circles in Fig. 2 represent the numerical results by means of the Monte-Carlo integration. We took 200 ensembles to calculate the expectation value. In the SU(2) case the numerical results agree well with the expression (21). Also, an analytical expression,

$$\lim_{\zeta \rightarrow 0} \lim_{\epsilon \rightarrow 0} \langle V_\epsilon^\dagger \rangle_\zeta = \left( 1 - g^4 \bar{\mu}^2 \frac{1}{2} L(0, 0) + g^8 \bar{\mu}^4 \frac{1}{24} L(0, 0)^2 \right) \exp \left[ -g^4 \bar{\mu}^2 \frac{1}{6} L(0, 0) \right], \quad (25)$$

can nicely fit the SU(3) results. In any case, it is obvious that the numerical results deviate from the analytical formula (18) substantially.

## B. Gauge Fields

In view of the tadpole results, one might have thought that the discrepancy is only minor. The deviation may look small, however, simply because the expectation value of non-singlet operators in color is exponentially suppressed

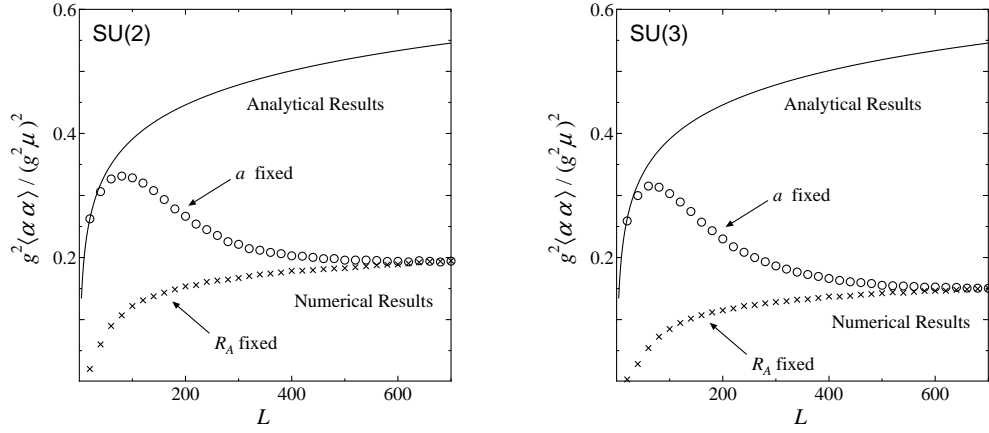


FIG. 3: Gauge field expectation value as a function of  $L$ . The analytical results are given by Eqs. (26) and (27). The parameter  $g^2\bar{\mu}a$  is fixed to be 0.17 for the  $a$ -fixed results and  $g^2\bar{\mu}a$  scales as  $0.17 \times 700/L$  for the  $R_A$ -fixed results. The left figure is for the SU(2) group and the right for the SU(3) group.

by the system size  $R_A$ . This fact becomes manifest once we consider some operators that contain a color singlet component.

Here, let us elucidate a more complicated situation, that is, the expectation value of gauge fields  $\langle\alpha\alpha\rangle$  (see Eq. (8) for our notation) which have a contribution from the color singlet. In this case the Gaussian integral is too tedious to accomplish, so we will rely on the numerical Monte-Carlo integration only. On the other hand, the analytical calculation with the path-ordering is still possible and it follows;

$$\langle\alpha\alpha\rangle = \frac{1}{g^2} (g^2\bar{\mu})^2 \sigma, \quad (26)$$

where

$$\sigma = \frac{1}{4L^2} \sum_{n_i=1-L/2}^{L/2} \frac{1}{2 - \cos(2\pi n_1/L) - \cos(2\pi n_2/L)} \simeq \frac{1}{4\pi} \ln(1.36L), \quad (27)$$

which does not depend on  $N_c$  at all and monotonically grows up with increasing  $L$ . We numerically find a constant 1.36 in the logarithm. This expression is, hence, singular both infraredly and ultravioletly. That is,  $\langle\alpha\alpha\rangle \rightarrow \infty$  whenever  $L \rightarrow \infty$ , which occurs in the limit of  $R_A \rightarrow \infty$  or in the limit of  $a \rightarrow 0$  (see Eq. (24)). More importantly, the analytical formula (26) and (27) claims that the infrared behavior as  $R_A \rightarrow \infty$  and the ultraviolet behavior as  $a \rightarrow 0$  are completely identical. This property is, however, no longer the case in the numerical results.

Figure 3 shows the results by the Monte-Carlo integration. The shape of  $g^2\langle\alpha\alpha\rangle/(g^2\bar{\mu})^2$  as a function of  $L$  clearly depends on whether  $R_A \propto L$  increases with  $a$  fixed or  $a \propto 1/L$  decreases with  $R_A$  fixed. In the case that  $a$  is fixed, the calculation goes just in the same way as in the previous subsection; we choose  $g^2\bar{\mu}a = 0.17$ . When we keep  $R_A$  fixed, we adjust the lattice spacing as  $g^2\bar{\mu}a = 0.17 \times 700/L$ , so that  $g^2\bar{\mu}a = 0.17$  for  $L = 700$ , which is completely equivalent to the procedure in Ref. [22]. Thus, the  $a$ -fixed curve and  $R_A$ -fixed curve should meet at  $L = 700$ , as is certainly the case in Fig. 3.

The numerical results hardly depend on  $N_c$ ; the left and right figures of Fig. 3 look almost the same, though the SU(3) results are slightly smaller than the SU(2) ones. The numerical calculation leads to  $g^2\langle\alpha\alpha\rangle/(g^2\bar{\mu})^2 = 0.194$  at  $L = 700$  for the SU(2) group, while the SU(3) group results in 0.150 at  $L = 700$ . In contrast to the tadpole case, the numerical data underestimate the expectation value that is  $g^2\langle\alpha\alpha\rangle/(g^2\bar{\mu})^2 = \alpha = 0.546$  in the analytical method. In the next section, we will discuss how we may be able to remedy this disastrous mismatch.

## VI. IMPROVEMENT

We can improve the situation by inserting the infinitesimal sheet in longitudinal extent in a way as sketched in Fig. 4. We denote the number of sheets by  $N_\eta$ . We note that  $N_\eta$  is *not* the longitudinal coordinate as in Ref. [24], but it is the number of slices within infinitesimal extent. Hence, all the numerical results we have seen so far correspond to  $N_\eta = 1$ . We can recover the full path-ordering in the  $N_\eta \rightarrow \infty$  limit.

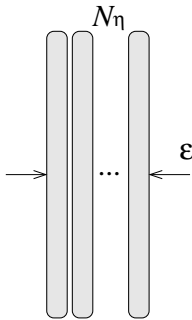


FIG. 4: Schematic picture of how to improve the numerical results. Each blob represents the two-dimensional sheet without longitudinal randomness. In the  $N_\eta \rightarrow \infty$  limit we can recover the full randomness structure in longitudinal extent which is infinitesimal in the  $\epsilon \rightarrow 0$  limit.

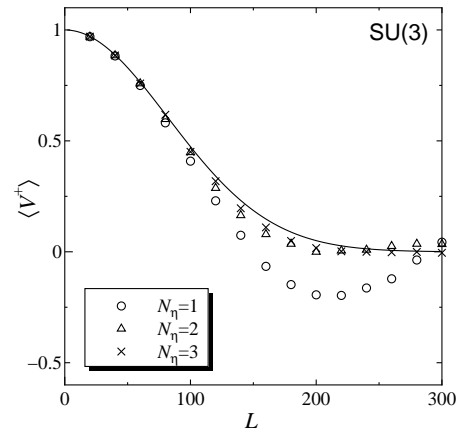


FIG. 5: Tadpole expectation value for the SU(3) case at  $N_\eta = 1$  (same as shown previously),  $N_\eta = 2$ , and  $N_\eta = 3$ .

For example, in the tadpole case, we shall modify the Gaussian integral in Eq. (20) into the form of

$$\langle V^\dagger \rangle_{N_\eta} = \prod_{n=1}^{N_\eta} \int [d\bar{\rho}_n] \exp \left[ ig \int d^2 \mathbf{y}_\perp G_0(\mathbf{x}_\perp - \mathbf{y}_\perp) \bar{\rho}_n(\mathbf{y}_\perp) \right] \exp \left[ - \int d^2 \mathbf{x}_\perp \frac{\text{tr}[\bar{\rho}_n(\mathbf{x}_\perp)^2]}{g^2(\bar{\mu}^2/N_\eta)} \right], \quad (28)$$

to retrieve the analytical results in the limit of  $N_\eta \rightarrow \infty$ . We have to divide  $\bar{\mu}^2$  by  $N_\eta$  to make it consistent with Eq. (10). It is, however, impossible to take the  $N_\eta \rightarrow \infty$  limit in the practical procedure. Instead, in this section let us focus only on  $N_\eta = 2$ ,  $N_\eta = 3$ , and  $N_\eta = 10$  to demonstrate the tendency of how the numerical outputs could move from the structureless  $N_\eta = 1$  results toward the analytical answer. We did calculate in the SU(2) case as well as in the SU(3) case, but we will present only the SU(3) results here, for the gauge group makes no qualitative difference.

The improvement works nicely for the tadpole expectation value as is evident in Fig. 5. The results at  $N_\eta = 2$  almost reproduces the analytical curve. So, the strategy to cure the pathology might seem promising.

However, the gauge field expectation value scarcely benefits from this improvement procedure. We show the results in Fig. 6 for the  $a$ -fixed calculation (left) and the  $R_A$ -fixed calculation (right). The improvement seems rather better for the infrared behavior with  $a$  fixed. The ultraviolet behavior with  $R_A$  fixed barely moves with increasing  $N_\eta$ . This is because the reference point for the  $R_A$ -fixed calculation is chosen at  $L = 700$  where the deviation between the analytical and numerical results is acute as perceived from Fig. 3. So,  $N_\tau$  must be comparable to  $\sim 700$  to achieve a nice deal of improvement for the  $R_A$ -fixed results. We would observe better convergence if  $g^2 \bar{\mu} a L$  is smaller than  $0.17 \times 700$  that we chose here.

## VII. DISCUSSIONS

From the comparison between the analytical and numerical outputs, we can learn an important lesson; the numerical implementation like Eq. (11) becomes worse and worse as we approach the continuum limit in the transverse plane. This is a sort of dilemma. We should insert more and more sheets along the longitudinal direction as in Fig. 4 when we make use of a finer lattice or a larger volume. Of course, the computation time increases as  $N_\eta$  gets larger because the number of the integration variables is proportional to  $N_\eta$  as seen in Eq. (28).

Our finding that the longitudinal structure in infinitesimal extent has a significant effect on the expectation value in the MV model is also important for the instability analyses in Ref. [24]. Because the instability takes place with respect to the longitudinal fluctuations, it is naturally expected that the proper treatment of longitudinal randomness should alter the quantitative features discussed in Ref. [24]. It is an intriguing question whether the instability would remain weak as concluded in Ref. [24] with longitudinal randomness taken into account. If not, the instability might be fast and strong enough to account for the early thermalization. We have to emphasize that our  $N_\eta$  is not the same as employed in Ref. [24] in which the authors introduced the longitudinal *coordinate* to solve the equation of motion in three-dimensional space, but did not store the random sheets within infinitesimal extent *in the initial condition*.

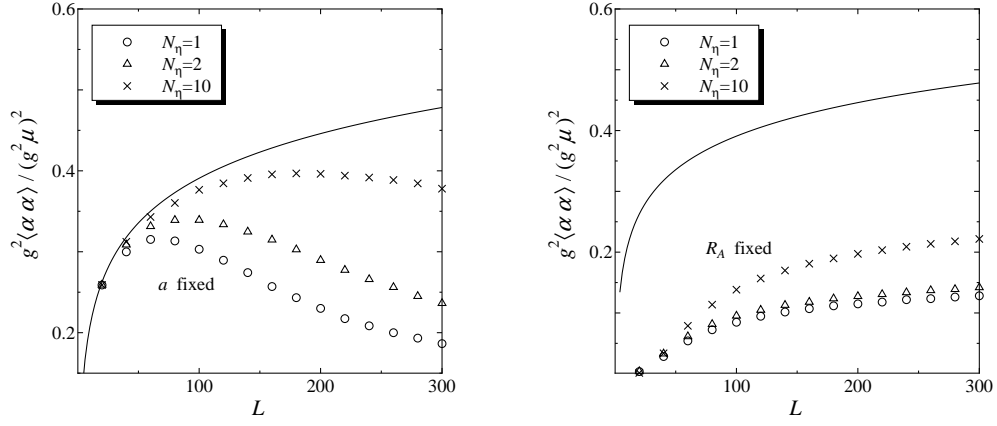


FIG. 6: Gauge field expectation value for the SU(3) case at  $N_\eta = 1$  (same as shown previously),  $N_\eta = 2$ , and  $N_\eta = 10$ . The convergence to the analytical answer is much slower than the tadpole case especially for larger  $L$ .

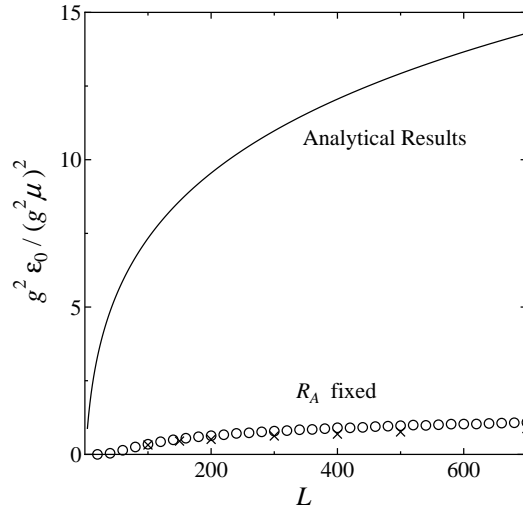


FIG. 7: Initial energy density in the analytical calculation shown by the solid curve and the numerical estimate shown by the open circles. The cross points represent the data presented in Ref. [22].

The vital difference lies in the fact that the number of the Monte-Carlo integration variables  $\bar{\rho}_n(\mathbf{x}_\perp)$  ( $n = 1, \dots, N_\eta$ ) becomes greater with increasing  $N_\eta$ .

Finally we shall apply our results to the comparison of the initial energy density between the analytical formula by Eq. (8) and what was reported in Ref. [22]. As we have discussed, the numerical formulation with the approximation (11) underestimates the gauge field expectation value by a factor  $0.546/0.15 = 3.64$ . Therefore, the initial energy density obtained in the numerical method is smaller than the analytical estimate by a factor  $3.64^2 = 13.2$ .

We plot the initial energy density in Fig. 7. It should be mentioned that, though the important message from Ref. [22] is that the initial energy density at  $\tau = 0$  is ill-defined and logarithmically divergent, our analytical calculation leads to a finite value with the infrared and ultraviolet cutoffs (i.e.  $a > 0$  and  $L < \infty$ ), which is just the same reason why the lattice discretized results are always finite. Of course, the analytical formula becomes logarithmically divergent in the limit of  $a \rightarrow 0$  or  $L \rightarrow \infty$ .

We note that our numerical estimate is close to the data calculated in the numerical simulation in Ref. [22] which is overlaid on Fig. 7 by the cross points. The small discrepancy should be explained by difference between the naive discretization and the lattice formulation in terms of the link variables. We should remark that Fig. 7 does not necessarily mean that the initial energy density *in the physical unit* has such huge mismatch. If the numerical method underestimates all the physical quantities, the chosen  $\bar{\mu}$  in the physical unit is accordingly larger than that in the analytical approach. Consequently, the mismatch could be in part compensated for by the choice of  $\bar{\mu}$ . We need to look carefully into the determination of  $\bar{\mu}$  from the analytical side in the future.



## Acknowledgments

The author thanks Teiji Kunihiro for useful conversations, Paul Romatschke for encouraging and helpful comments, and Raju Venugopalan for communications.

- 
- [1] L. D. McLerran and R. Venugopalan, Phys. Rev. D **49**, 2233 (1994) [arXiv:hep-ph/9309289]; 3352 (1994) [arXiv:hep-ph/9311205]; D **50**, 2225 (1994) [arXiv:hep-ph/9402335].
  - [2] For reviews, see: E. Iancu and R. Venugopalan, arXiv:hep-ph/0303204; E. Iancu, A. Leonidov and L. McLerran, arXiv:hep-ph/0202270.
  - [3] L. V. Gribov, E. M. Levin and M. G. Ryskin, Phys. Rept. **100**, 1 (1983).
  - [4] A. M. Stasto, K. J. Golec-Biernat and J. Kwiecinski, Phys. Rev. Lett. **86**, 596 (2001) [arXiv:hep-ph/0007192].
  - [5] E. Iancu, K. Itakura and L. McLerran, Nucl. Phys. A **724**, 181 (2003) [arXiv:hep-ph/0212123].
  - [6] Y. V. Kovchegov, Phys. Rev. D **54**, 5463 (1996) [arXiv:hep-ph/9605446].
  - [7] J. Jalilian-Marian, A. Kovner, L. D. McLerran and H. Weigert, Phys. Rev. D **55**, 5414 (1997) [arXiv:hep-ph/9606337].
  - [8] J. P. Blaizot, F. Gelis and R. Venugopalan, Nucl. Phys. A **743**, 13 (2004) [arXiv:hep-ph/0402256].
  - [9] J. P. Blaizot, F. Gelis and R. Venugopalan, Nucl. Phys. A **743**, 57 (2004) [arXiv:hep-ph/0402257].
  - [10] F. Gelis and Y. Mehtar-Tani, Phys. Rev. D **73**, 034019 (2006) [arXiv:hep-ph/0512079].
  - [11] Y. Hatta, Nucl. Phys. A **781**, 104 (2007) [arXiv:hep-ph/0607126].
  - [12] K. Fukushima and Y. Hidaka, JHEP **0706**, 040 (2007) [arXiv:0704.2806 [hep-ph]].
  - [13] A. Kovner, L. D. McLerran and H. Weigert, Phys. Rev. D **52**, 3809 (1995) [arXiv:hep-ph/9505320]; 6231 (1995) [arXiv:hep-ph/9502289].
  - [14] M. Gyulassy and L. D. McLerran, Phys. Rev. C **56**, 2219 (1997) [arXiv:nucl-th/9704034].
  - [15] Y. V. Kovchegov and D. H. Rischke, Phys. Rev. C **56**, 1084 (1997) [arXiv:hep-ph/9704201].
  - [16] R. J. Fries, J. I. Kapusta and Y. Li, arXiv:nucl-th/0604054.
  - [17] K. Fukushima, Phys. Rev. C **76**, 021902 (2007) [arXiv:0704.3625 [hep-ph]].
  - [18] A. Krasnitz and R. Venugopalan, Nucl. Phys. B **557**, 237 (1999) [arXiv:hep-ph/9809433]; Phys. Rev. Lett. **84**, 4309 (2000) [arXiv:hep-ph/9909203]; **86**, 1717 (2001) [arXiv:hep-ph/0007108].
  - [19] A. Krasnitz, Y. Nara and R. Venugopalan, Phys. Rev. Lett. **87**, 192302 (2001) [arXiv:hep-ph/0108092]; Nucl. Phys. A **717**, 268 (2003) [arXiv:hep-ph/0209269]; **727**, 427 (2003) [arXiv:hep-ph/0305112].
  - [20] T. Lappi, Phys. Rev. C **67**, 054903 (2003) [arXiv:hep-ph/0303076].
  - [21] T. Lappi and L. McLerran, Nucl. Phys. A **772**, 200 (2006) [arXiv:hep-ph/0602189].
  - [22] T. Lappi, Phys. Lett. B **643**, 11 (2006) [arXiv:hep-ph/0606207].
  - [23] K. Fukushima, F. Gelis and L. McLerran, Nucl. Phys. A **786**, 107 (2007) [arXiv:hep-ph/0610416].
  - [24] P. Romatschke and R. Venugopalan, Phys. Rev. Lett. **96**, 062302 (2006) [arXiv:hep-ph/0510121]; Phys. Rev. D **74**, 045011 (2006) [arXiv:hep-ph/0605045].